

Smooth and Time-Optimal Trajectory Planning for Industrial Manipulators along Specified Paths

D. Constantinescu,* E. A. Croft
*Industrial Automation Laboratory,
Department of Mechanical Engineering,
University of British Columbia,
Vancouver, BC, Canada V6T 1Z4
e-mail: daniela@mech.ubc.ca*

Received January 2, 1999; accepted January 21, 2000

This article presents a method for determining smooth and time-optimal path constrained trajectories for robotic manipulators and investigates the performance of these trajectories both through simulations and experiments. The desired smoothness of the trajectory is imposed through limits on the torque rates. The third derivative of the path parameter with respect to time, the pseudo-jerk, is the controlled input. The limits on the actuator torques translate into state-dependent limits on the pseudo-acceleration. The time-optimal control objective is cast as an optimization problem by using cubic splines to parametrize the state space trajectory. The optimization problem is solved using the flexible tolerance method. The experimental results presented show that the planned smooth trajectories provide superior feasible time-optimal motion. © 2000 John Wiley & Sons, Inc.

1. INTRODUCTION

The need for increased productivity in path-following industrial robotic applications has been commonly addressed in the literature by determining path-constrained time-optimal motions (PCTOM) while accounting for actuator torque limits¹⁻³. In these formulations, the joint actuator torques are the controlled inputs and the open loop control

schemes result in bang-bang or bang-singular-bang controls.^{1,3,4}

PCTOM trajectories compute the maximum velocity achievable at the robot tip while still following the prescribed path. However, implementation of PCTOM in physical manipulators has drawbacks, such as joint oscillations due to finite joint stiffness and overshoot of the nominal torque limits due to unmodelled actuator dynamics. The resultant extra strain on the robot actuators could cause them to fail frequently,⁵ reducing the productivity of the entire workcell.

*To whom all correspondence should be addressed.

At the trajectory planning level, a number of different techniques have been devised to address the problem of discontinuous actuator torques. A modified cost function, such as time-joint torques² or time-square of joint torques,⁶ can be used to smooth the controls and improve the tracking accuracy, at the expense of motion time.

Another way of smoothing the controls is to parametrize the path by using functions that are at least C^2 continuous, i.e., continuous in acceleration. Cubic splines used for path parametrization with time as the cost function⁷ result in trajectories that have continuous joint accelerations. However, the limits on the joint variables are very conservative, since they remain constant over the entire work space. Incorporating the actuator dynamics in this problem formulation⁸ transforms the actuator voltages into the limited controlled inputs. The optimal trajectory is bang-bang in the new controls and the actuator torques are no longer limited. Also, the case of singular controls is not considered since they can be avoided by an appropriate selection of the path³ or by convexifying the set of admissible controls.⁹

In this article, a method is presented for determining time-optimal path-constrained motions subject to limits on the actuator torques and the first derivative of actuator torques, or "torque rates." The resulting trajectories will be called smooth path-constrained time-optimal motions (SPCTOM) to distinguish them from the path-constrained time-optimal motions (PCTOM), which do not consider torque rate limits.

The actuator torque rate limits are imposed in view of the fact that unlimited changes in torque can cause highly jerky motion and severe vibrations in the arm that may lead to the failure of the actuators themselves. Moreover, they are used as a means to compensate for structure flexibility and inaccuracies in the robot model. This is a desired feature in industrial applications, where the robot model is not readily available. Therefore, the benefit of the SPCTOM trajectories is that they better characterize the dynamic limitations of a robot system and, hence, are suited for direct implementation on a commercial robot using nonspecialized industrial controllers.

Geometric limits on robot motion, such as obstacles and joint limits, are not addressed herein, since the motion is path-constrained. That is, only the trajectory planning problem is considered. The path is either imposed by the application itself or a time-optimal path can be determined as in ref. 10: Under the assumption that the desired path is

smooth, an initial guess is generated using splines and the optimal path is found through an unconstrained parameter optimization. The cost function is composed of the motion time along the path plus penalty terms corresponding to obstacles and joint limits.

2. SMOOTH PATH-CONSTRAINED TIME-OPTIMAL MOTIONS

2.1. Problem Formulation

The problem of SPCTOM planning can be stated as

$$\min_{\mathbf{r} \in \Omega} J = \int_0^{t_f} 1 dt, \quad (1)$$

subject to the manipulator dynamics,

$$\mathbf{M}(\mathbf{q})\ddot{\mathbf{q}} + \dot{\mathbf{q}}^T \mathbf{G}(\mathbf{q})\dot{\mathbf{q}} + \mathbf{G}(\mathbf{q}) = \mathbf{T}, \quad (2)$$

the boundary conditions,

$$\begin{aligned} \mathbf{q}(0) = \mathbf{q}_0; \quad \mathbf{q}(t_f) = \mathbf{q}_f; \quad \dot{\mathbf{q}}(0) = \dot{\mathbf{q}}(t_f) = 0; \\ \ddot{\mathbf{q}}(0) = \ddot{\mathbf{q}}(t_f) = 0, \end{aligned} \quad (3)$$

the path constraints,

$$\mathbf{r} = \mathbf{r}(s), \quad (4)$$

the actuator torque limits,

$$\mathbf{T}_{\min} \leq \mathbf{T} \leq \mathbf{T}_{\max}, \quad (5)$$

and the actuator torque rate limits:

$$\dot{\mathbf{T}}_{\min} \leq \dot{\mathbf{T}} \leq \dot{\mathbf{T}}_{\max}, \quad (6)$$

where n is the number of degrees of freedom of the manipulator. Furthermore, $\mathbf{q} \in \mathbf{R}^n$ is the vector of joint positions, $\mathbf{T} \in \mathbf{R}^n$ is the vector of actuator torques, $\dot{\mathbf{T}} \in \mathbf{R}^n$ is the vector of torque rates, $\mathbf{M}(\mathbf{q}) \in \mathbf{R}^{n \times n}$ is the inertia matrix of the manipulator, $\mathbf{C}(\mathbf{q}) \in \mathbf{R}^{n \times n \times n}$ is a third-order tensor representing the coefficients of the centrifugal and Coriolis forces, $\mathbf{G}(\mathbf{q}) \in \mathbf{R}^n$ is the vector of gravity terms, and $\mathbf{r} \in \mathbf{R}^3$ is a C^1 continuous curve parametrized by s , which may be, for example, the arc length. To simplify the dynamics, viscous and static friction terms have been neglected. However, as shown in the experiments in Section 5, the imposition of suitable torque rate limits compensates for these and other model inaccuracies.

In the above formulation, the torque rates represent the bounded controls. Since the Lagrangian form of the robot dynamics incorporates only the actuator torques, the third-order dynamics is required. Differentiation of (2) with respect to time results in

$$\mathbf{M}(\mathbf{q})\ddot{\mathbf{q}} + \dot{\mathbf{M}}(\mathbf{q})\dot{\mathbf{q}} + \dot{\mathbf{q}}^T \mathbf{C}(\mathbf{q})\dot{\mathbf{q}} - \dot{\mathbf{q}}^T \dot{\mathbf{C}}(\mathbf{q})\dot{\mathbf{q}} + \dot{\mathbf{q}}^T \mathbf{C}(\mathbf{q})\ddot{\mathbf{q}} + \dot{\mathbf{G}}(\mathbf{q}) = \dot{\mathbf{T}}. \quad (7)$$

Equation (7) is taken as the dynamics of the system, with $\dot{\mathbf{T}}$ representing the n -dimensional bounded controls.

2.2. Path Constraints

The dynamic system described by Eq. (7) has $3n$ degrees of freedom. However, the path constraints (4) parametrize the end-effector tip position by a single parameter s , reducing the order of the system to 3.

To obtain the torque rate bounds for the reduced order system, the joint jerk is computed as

$$\ddot{\mathbf{q}} = \mathbf{q}''' \dot{s}^3 + 3 \cdot \mathbf{q}'' \cdot \dot{s} \ddot{s} + \mathbf{q}' \ddot{s}, \quad (8)$$

where

$$\mathbf{q}''' = \mathbf{J}^{-1} \cdot \left(\mathbf{r}''' - \frac{d^2 \mathbf{J}}{ds^2} \cdot \mathbf{q}' - 2 \cdot \frac{d\mathbf{J}}{ds} \cdot \mathbf{q}'' \right), \quad (9)$$

$$\mathbf{r}''' = \frac{d^2 \mathbf{J}}{ds^2} \cdot \mathbf{q}' + 2 \cdot \frac{d\mathbf{J}}{ds} \cdot \mathbf{q}'' + \mathbf{J} \cdot \mathbf{q}''', \quad (10)$$

with \mathbf{r} being the end-effector position and orientation, \mathbf{J} being the Jacobian of the forward kinematics map, and $'$ denoting the derivative with respect to the path parameter. Substituting Eqs. (7) and (8) into Eq. (6) yields

$$\dot{\mathbf{T}}_{\min} \leq \mathbf{a}(s) \cdot \ddot{s} + \mathbf{b}(s) \cdot \dot{s} \cdot \ddot{s} + \mathbf{c}(s) \cdot \dot{s}^3 + \mathbf{d}(s) \cdot \dot{s} \leq \dot{\mathbf{T}}_{\max}, \quad (11)$$

where

$$\mathbf{a}_{n \times 1}(s) = \mathbf{M} \cdot \mathbf{q}', \quad (12)$$

$$\mathbf{b}_{n \times 1}(s) = 3 \cdot \mathbf{M} \cdot \mathbf{q}'' + \frac{d\mathbf{M}}{ds} \cdot \mathbf{q}' + 2 \cdot \mathbf{q}'^T \cdot \mathbf{C} \cdot \mathbf{q}', \quad (13)$$

$$\begin{aligned} \mathbf{c}_{n \times 1}(s) = & \mathbf{M} \cdot \mathbf{q}''' + \frac{d\mathbf{M}}{ds} \cdot \mathbf{q}'' + \mathbf{q}''^T \cdot \mathbf{C} \cdot \mathbf{q}' \\ & + \mathbf{q}'^T \cdot \frac{d\mathbf{C}}{ds} \cdot \mathbf{q}' + \mathbf{q}'^T \cdot \mathbf{C} \cdot \mathbf{q}'', \end{aligned} \quad (14)$$

$$\mathbf{d}_{n \times 1}(s) = \frac{d\mathbf{G}}{ds} \cdot \dot{s}. \quad (15)$$

The matrices $d\mathbf{M}/ds$ and $d\mathbf{G}/ds$ and the third-order tensor $d\mathbf{C}/ds$ are robot dependent.

As shown in Section 2.3, the torque rate bounds provide constraints on the admissible states for the robot. However, the torque bounds derived in refs. 3 and 11 are still required, since, as the torque rate bounds become very large, the torque bounds become the limiting constraint. For infinite torque rates, the problem returns to PCTOM.

Following ref. 3, the actuator torque bounds for the reduced order system are obtained substituting the path constraints (4) and Eq. (2) into Eq. (5):

$$\mathbf{T}_{\min} \leq \mathcal{A}(s) \cdot \ddot{s} + \mathcal{B}(s) \cdot \dot{s}^2 + \mathcal{C}(s) \leq \mathbf{T}_{\max}, \quad (16)$$

where

$$\mathcal{A}_{n \times 1}(s) = \mathbf{M} \cdot \mathbf{q}', \quad (17)$$

$$\mathcal{B}_{n \times 1}(s) = \mathbf{M} \cdot \mathbf{q}'' + \mathbf{q}'^T \cdot \mathbf{C} \cdot \mathbf{q}', \quad (18)$$

$$\mathcal{C}_{n \times 1}(s) = \mathbf{G}. \quad (19)$$

2.3. Torque Limits

As discussed in ref. 3, for each value of the path parameter s , the actuator torque bounds (16) translate into a polygonal feasible region in the \dot{s}^2 - \ddot{s} plane. Such a region is shown schematically in Figure 1 for a 3-dof manipulator. Analytically, the actuator torque bounds translate into limits on the pseudo-velocity and the pseudo-acceleration:

$$\dot{s} \leq \dot{s}_{\max, T}(s) \quad (20)$$

$$\ddot{s}_{\min, T}(s, \dot{s}) \leq \ddot{s} \leq \ddot{s}_{\max, T}(s, \dot{s}). \quad (21)$$

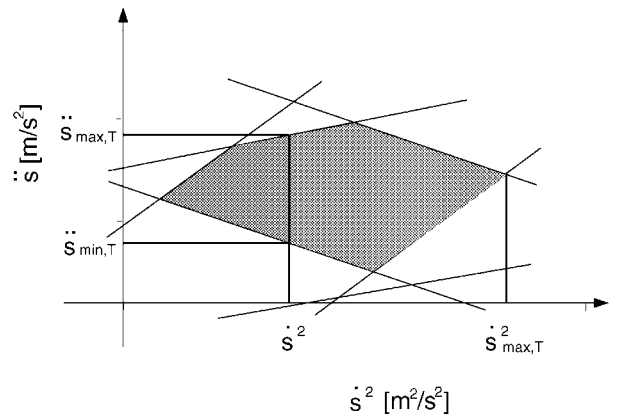


Figure 1. Admissible region in the \dot{s}^2 - \ddot{s} plane, after ref. 3.

The subscript T is used to discriminate the pseudo-velocity and pseudo-acceleration bounds due to the torque constraints (16) from those due to the torque rate constraints (11), which will be denoted with the subscript J .

The curve $\dot{s}_{\max,T}(s)$ as represented in the $s-\dot{s}$ phase plane is called the *velocity limit curve* (VLC) and it represents an upper bound for any feasible trajectory in this plane. The constraints on the pseudo-velocity and pseudo-acceleration due to the actuator torque limits are computed as discussed in ref. 3.

2.4. Torque Rate Limits

A similar approach can be used to determine the pseudo-velocity, pseudo-acceleration, and pseudo-jerk bounds due to the torque rate limits. Thus, for given values of the path parameter s and pseudo-velocity \dot{s} , the torque rate bounds (11) form a polygonal feasible region in the $\ddot{s} - \ddot{\ddot{s}}$ plane (such as the one shown schematically in Fig. 2 for a 3-dof manipulator). Analytically, the torque rate bounds translate into pseudo-acceleration and pseudo-jerk limits in the $\ddot{s} - \ddot{\ddot{s}}$ plane:

$$\ddot{s}_{\min,J}(s, \dot{s}) \leq \ddot{s} \leq \ddot{s}_{\max,J}(s, \dot{s}) \quad (22)$$

$$\ddot{\ddot{s}}_{\min}(s, \dot{s}, \ddot{s}) \leq \ddot{\ddot{s}} \leq \ddot{\ddot{s}}_{\max}(s, \dot{s}, \ddot{s}) \quad (23)$$

and a constraint on the pseudo-velocity in the $\dot{s} - \ddot{\ddot{s}}$ space

$$\dot{s} \leq \dot{s}_{\max,J}(s), \quad (24)$$

where $\dot{s}_{\max,J}(s)$ is defined as the pseudo-velocity value for which the admissible region in the $\ddot{s} - \ddot{\ddot{s}}$

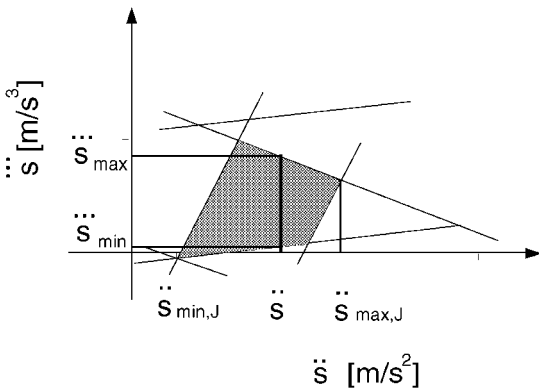


Figure 2. Admissible region in the $\ddot{s}-\ddot{\ddot{s}}$ plane.

plane reduces to a point

$$\ddot{\ddot{s}}_{\min,J}(s, \dot{s}_{\max,J}) = \ddot{\ddot{s}}_{\max,J}(s, \dot{s}_{\max,J}). \quad (25)$$

After performing the calculations, the pseudo-jerk and pseudo-acceleration limits result as

$$\ddot{\ddot{s}}_{\min}(s, \dot{s}, \ddot{s}) = \max_i \left\{ \min_{\dot{T}_i} \left(\frac{\dot{T}_i - c_i^* - b_i^* \ddot{s}}{a_i} \right) \right\}, \quad i = 1, \dots, n, \quad (26)$$

$$\ddot{\ddot{s}}_{\max}(s, \dot{s}, \ddot{s}) = \min_i \left\{ \max_{\dot{T}_i} \left(\frac{\dot{T}_i - c_i^* - b_i^* \ddot{s}}{a_i} \right) \right\}, \quad i = 1, \dots, n, \quad (27)$$

and

$$\begin{aligned} \ddot{s}_{\min,J}(s, \dot{s}) &= \max_{i,j} \left\{ \min_{\dot{T}_i, \dot{T}_j} \left(\frac{a_j(\dot{T}_i - c_i^*) - a_i(\dot{T}_j - c_j^*)}{a_j b_i^* - a_i b_j^*} \right) \right\}, \\ i, j &= 1, \dots, n, \end{aligned} \quad (28)$$

$$\begin{aligned} \ddot{s}_{\max,J}(s, \dot{s}) &= \min_{i,j} \left\{ \max_{\dot{T}_i, \dot{T}_j} \left(\frac{a_j(\dot{T}_i - c_i^*) - a_i(\dot{T}_j - c_j^*)}{a_j b_i^* - a_i b_j^*} \right) \right\}, \\ i, j &= 1, \dots, n, \end{aligned} \quad (29)$$

and the pseudo-velocity limit can be computed by a numerical search.

2.5. Admissible States

In the formulation of the SPCTOM problem proposed herein, the torque rate limits are imposed as a means for adjusting the smoothness of the trajectory. Hence, they are independent of the actuator torque limits. This independence is reflected in the state space, as shown in Figure 3. In this figure, the actuator torque and torque rate constraints for the first three joints of the SCORBOT ER VII robot (Fig. 6, Table I) are plotted together in state space for the three example torque rate limits in Table II.

This independence of the actuator torque and torque rate limits is reflected in a new constraint on the pseudo-velocity,

$$\dot{s} \leq \min\{\dot{s}_{\max,T}(s), \dot{s}_{\max,J}(s)\}, \quad (30)$$

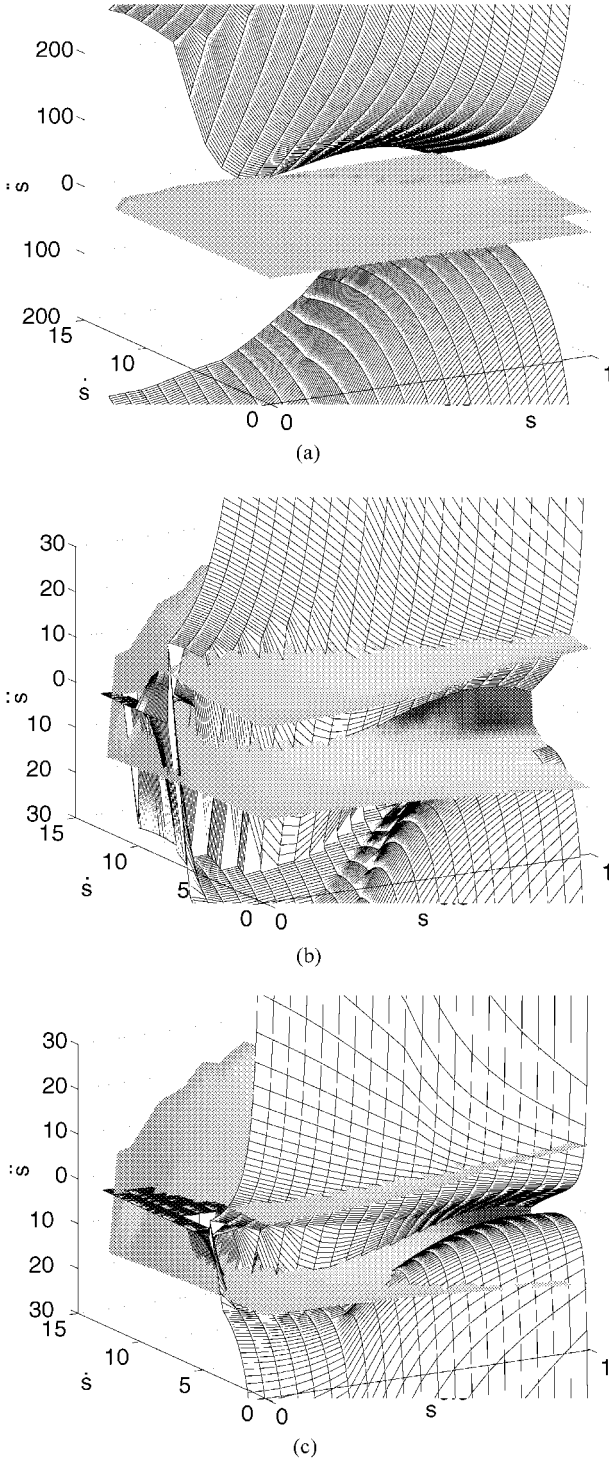


Figure 3. Admissible states in the s - \dot{s} - \ddot{s} space.

Table I. SCORBOT ER VII estimated kinematic and dynamic parameters.

Link	θ [rad]	d [m]	a [m]	α [rad]
1	$\theta_1 = 0$	$d_1 = 0.3585$	$a_1 = 0.05$	$\alpha_1 = -\frac{\pi}{2}$
2	$\theta_2 = 0$	$d_2 = -0.037$	$a_2 = 0.30$	$\alpha_2 = 0$
3	$\theta_3 = 0$	$d_3 = 0.0$	$a_3 = 0.25$	$\alpha_3 = 0$
Link	Mass [kg]	I_x [kgm ²]	I_y [kgm ²]	I_z [kgm ²]
1	$m_1 = 0.0$	$I_{x1} = 0.00$	$I_{y1} = 0.05$	$I_{z1} = 0.0$
2	$m_2 = 6.6$	$I_{x2} = 0.10$	$I_{y2} = 0.60$	$I_{z2} = 0.6$
3	$m_3 = 4.2$	$I_{x3} = 0.02$	$I_{y3} = 0.20$	$I_{z3} = 0.3$

and a new constraint on the pseudo-acceleration,

$$\begin{aligned} & \max\{\ddot{s}_{\min,T}(s), \ddot{s}_{\min,J}(s)\} \\ & \leq \ddot{s} \leq \min\{\ddot{s}_{\max,T}(s), \ddot{s}_{\max,J}(s)\}. \end{aligned} \quad (31)$$

Equation (30) defines a global velocity limit curve, called the *smooth motion velocity limit curve* (SMVLC). In the $s - \dot{s}$ plane, the SMVLC is an upper bound on any feasible trajectory. The SMVLC can be computed at each point along the path by a line search using bisection (the searched domain is limited from zero to $\dot{s}_{\max,T}(s)$).

The SMVLC corresponding to the three examples in Table II are plotted in Figure 4. As shown in this figure, the SMVLC is determined by a combination of both actuator torque and torque rate limits. Depending on the restrictions of the torque rate limits, they can determine the SMVLC almost entirely, as shown in the third example, or they can

Table II. Imposed actuator torque and torque rate bounds for the SCORBOT ER VII.

Torque limits	High torque rate limits	Medium torque rate limits	Low torque rate limits
Example 1	Example 2	Example 3	
T [Nm]	\dot{T}_1 [Nm/s]	\dot{T}_2 [Nm/s]	\dot{T}_3 [Nm/s]
$T_1 = 10$	$\dot{T}_{11} = 1000$	$\dot{T}_{12} = 100$	$\dot{T}_{13} = 10$
$T_2 = 10$	$\dot{T}_{21} = 1000$	$\dot{T}_{22} = 100$	$\dot{T}_{23} = 10$
$T_3 = 10$	$\dot{T}_{31} = 1000$	$\dot{T}_{32} = 100$	$\dot{T}_{33} = 10$

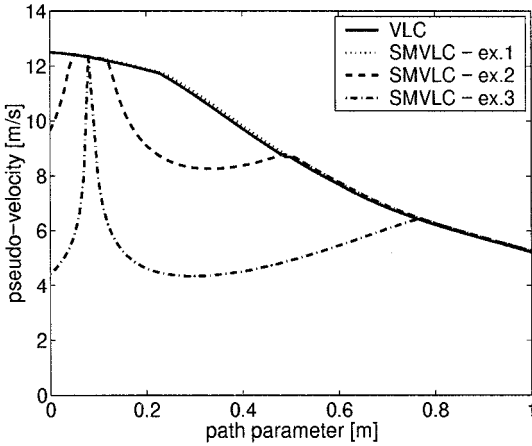


Figure 4. SMVLC for different actuator torque rate limits.

have little influence on it, as shown in the first example.

2.6. System Dynamics

The states of the reduced system are $\mathbf{x} = (s \dot{s} \ddot{s})^T$, while \ddot{s} is the scalar control u . The SPCTOM planning problem is reformulated as

$$\min_u J = \int_0^{t_f} 1 dt, \tag{32}$$

subject to the system dynamics

$$\dot{\mathbf{x}} = \mathbf{f}(\mathbf{x}, u) = [x_2 \quad x_3 \quad u]^T, \tag{33}$$

the boundary conditions:

$$\begin{aligned} \mathbf{x}_0 &= (s_0 \quad \dot{s}_0 \quad \ddot{s}_0)^T \\ \mathbf{x}_f &= (s_f \quad \dot{s}_f \quad \ddot{s}_f)^T, \end{aligned} \tag{34}$$

the state inequality constraints (30) and (31), and the state-dependent control inequality constraints (23).

This reformulation shows that the SPCTOM problem is a time-optimal control (TOC) problem for a first-order linear system with nonlinear state and control inequality constraints and preimposed initial and final states. Moreover, Equations (23), (30), and (31) emphasize that the state and control constraints are independently active, since the controls are limited only by the torque rates, while the states are limited by both the torque rates and the actuator torques.

3. SOLUTION OF THE SPCTOM

TOC problems similar to the SPCTOM above have been solved either by applying Pontryagin’s Maximum Principle (PMP) to derive the necessary conditions for optimality and then using multiple shooting methods to solve the resulting two point boundary value problem (TPBVP)¹² or by a search for the switching points, using either dynamic programming¹¹ or specific algorithms.¹⁻³

Two difficulties arise in the application of these approaches in the present case. First, the complexity of the dynamic programming algorithms grows exponentially with the phase space dimension, rendering the method infeasible for more than two dimensions. As defined, the SPCTOM problem has a three-dimensional phase space. Second, the other two approaches (based on PMP and the search for the switching points) depend on the bang-bang or bang-singular-bang structure of the optimal controls. This structure has been proven using results from optimal control theory (OCT) regarding systems with state dependent control constraints.¹³ However, no results have been proven using OCT concerning the necessary optimality conditions for systems with state and control constraints which are independently active. Thus, for the SPCTOM problem, it is not guaranteed that the optimal controls are bang-bang or bang-singular-bang.

To resolve these difficulties, the SPCTOM trajectory planning problem is analyzed and solved herein in the s - \dot{s} phase plane. The motivation is that in this plane both trajectory end-points are fixed, while in the time domain the final point is free. Thus, the TOC problem lends itself to a nonlinear parameter optimization in this phase plane. The motion time is computed as

$$t(s) = \int_{s_0}^{s_f} \frac{ds}{\dot{s}}, \tag{35}$$

where s_0 and s_f are the initial and the final values of the path parameter, respectively. Therefore, the SPCTOM in the s - \dot{s} phase plane is the smooth curve that minimizes $t(s)$ over the curve while not violating actuator torque and/or torque rate limits.

In view of the above, the optimal motion is determined by an optimization of a base trajectory. A set of cubic splines with preselected knot-point locations are chosen as the base trajectory for the optimization. Cubic polynomials have been selected to approximate the SPCTOM because they are the lowest degree polynomials that result in a smooth

curve, i.e., continuous and differentiable everywhere. The location of the knots along the path have been chosen to be the same as the location of the switching points of the PCTOM (Fig. 5). Since the PCTOM represents the limit for SPCTOM, these switching points are, in the limit, the same for SPCTOM and provide a reasonable estimate for the location of the SPCTOM switching points along the parametrized path.

Extra knot-points could be chosen; however, the number of the PCTOM trajectory switching points could be high and the addition of extra knots would significantly increase the number of optimization variables. Therefore, extra knots will be inserted only when the corresponding PCTOM trajectory has one single switching point. In this case the increase in computational time is negligible while a trajectory parametrization by only two splines could be inadequate.

This strategy is supported by simulations which have shown that doubling the number of knots improves the SPCTOM motion time by around 3–6% for trajectories with five switching points and by 10–17% for trajectories with only one switching point. The larger decrease in motion time is for trajectories with larger jerks.¹⁴

The variables of the optimization are the end-effector pseudo-velocities at the preselected knot-points along the path and the slopes of the trajectory in the s - \dot{s} phase plane at the path end-points. These variables control the motion time: the higher the knot-points over the whole trajectory (as located

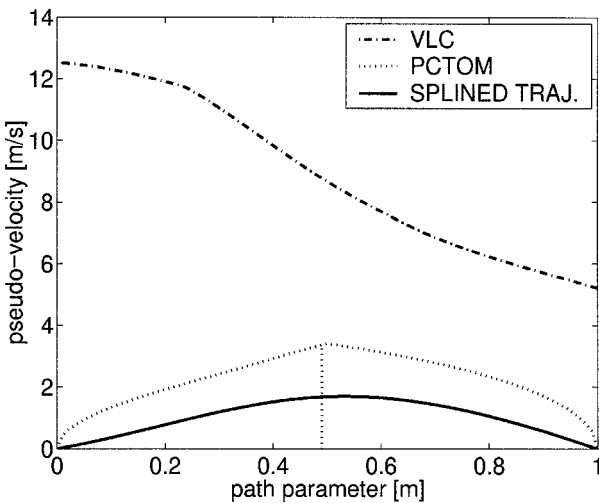


Figure 5. Switching points of the PCTOM (dotted line) and a sample splined trajectory (solid line).

in the phase plane), the shorter the motion time. On the other hand, the end slopes control the speed at which the actuator torques leave or approach their static equilibrium values. Therefore, steeper slopes also result in faster motion.

Thus, the vector of optimization variables, \mathbf{x} , is defined as the parameter set,

$$\mathbf{x} = \left(\begin{array}{cccc} \left(\frac{d\dot{s}}{ds} \right)_0 & \dot{s}_1 & \dots & \dot{s}_p & \left(\frac{d\dot{s}}{ds} \right)_f \\ \left(\frac{d\dot{s}}{ds} \right)_{m,0} & \dot{s}_{m,1} & & \dot{s}_{m,p} & \left(\frac{d\dot{s}}{ds} \right)_{m,f} \end{array} \right)^T, \quad (36)$$

where the values with the index m correspond to the limiting PCTOM (the dotted line in Fig. 5), while the other values correspond to the splined trajectory (the solid line). These variables are normalized since the end slopes vary over a much wider range than the pseudo-velocities.

The optimal trajectory results from splining cubic polynomials in the s - \dot{s} phase plane based on the optimized parameters \mathbf{x}^* . The trajectory must be within actuator torque and torque rate limits and take minimum time. The actuator torque and torque rate constraints in Eqs. (16) and (11) thus become

$$g_{4(i-1)+1}(\mathbf{x}) = 1 - \max_{\dot{s}(s)} \frac{T_i}{T_{\max,i}}, \quad (37)$$

$$g_{4(i-1)+2}(\mathbf{x}) = 1 - \max_{\dot{s}(s)} \frac{T_i}{T_{\min,i}}, \quad (38)$$

$$g_{4(i-1)+3}(\mathbf{x}) = 1 - \max_{\dot{s}(s)} \frac{\dot{T}_i}{\dot{T}_{\max,i}}, \quad (39)$$

$$g_{4(i-1)+4}(\mathbf{x}) = 1 - \max_{\dot{s}(s)} \frac{\dot{T}_i}{\dot{T}_{\min,i}}, \quad (40)$$

for $i = 1, \dots, n$. By this definition, whenever any of the actuator torques and/or torque rates exceeds its limits, the respective constraint becomes negative. Moreover, by enforcing the actuator torque and torque rate constraints directly, rather than the state and control constraints, the computations are greatly simplified.

As formulated, the optimization is solved using the flexible tolerance method (FTM).¹⁵ There are two reasons for choosing this method. First, the derivatives of the constraints and the cost function, i.e., motion time, are not available. Second, the FTM keeps the search close to the boundary of the admis-

sible region and can find a minimum that lies exactly on the boundary. The details of the FTM are discussed in the Appendix and further details on its implementation for solving the SPCTOM problem are presented in ref. 14.

4. SIMULATIONS

The method for determining optimal SPCTOM has been implemented in MATLAB¹⁶ and simulations are performed considering only the positional *dof* of the SCORBOT ER VII robot in the Industrial Automation Laboratory (IAL) at the University of British Columbia (UBC) (Fig. 6). Thus, for the simulations performed here, the robot is an elbow manipulator with the DH parameters and the estimated masses and inertias given in Table I.

The actuator torque limits are the same for all the three examples given in this paper, while the limits on the torque rates are different, as successively shown in Table II.

4.1. Planning Performance

To determine the influence of the trajectory smoothness on the motion time, a straight line in the robot work space is chosen as the preimposed path. In parametric form, the path is given as

$$\begin{aligned}x(s) &= 0.4 \\y(s) &= 0.3s - 0.1 \\z(s) &= 0.2s + 0.3 \\s &= 0, \dots, 1.\end{aligned}\quad (41)$$

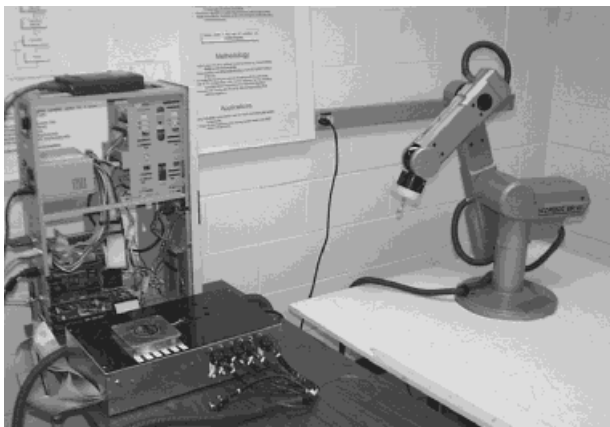


Figure 6. The SCORBOT ER VII robot.

The resulting optimal trajectories for the different limits on the torque rates are shown in Figures 7, 8, and 9, respectively, by solid lines. The dashed lines represent the time-optimal trajectory considering only torque limits (PCTOM). The dotted lines are the smooth motion velocity limit curves (SMVLC), i.e., the velocity limit curves determined considering both torque and torque rate limits. The corresponding actuator torques and torque rates are also plotted in these figures.

While the PCTOM takes 0.59 s, the SPCTOM takes 0.7 s in the first example. Here, the limits on the torque rates were very high (infeasible) and the trajectory is determined by the limits on the actuator torques. In the ideal case, both trajectories should yield the same motion times; however, there are two reasons for the increase in motion time for SPCTOM: (i) the limited parametrization chosen in the s - \dot{s} phase plane and (ii) the significant decrease in peak torque rates for SPCTOM (solid lines) compared to PCTOM (dotted lines), as shown in the semi-log-scale plot in Figure 10.

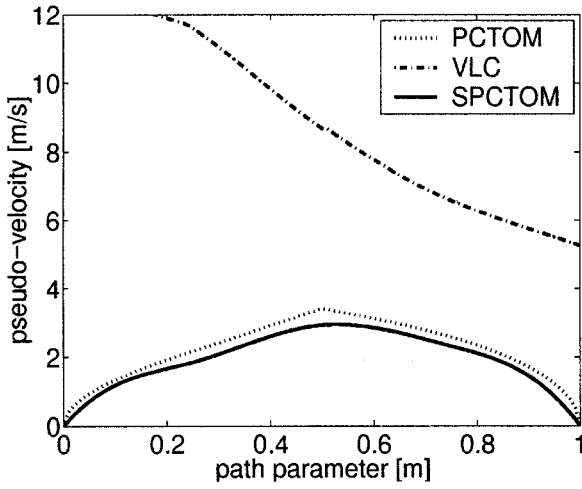
In examples 2 and 3, the more feasible limits on the torque rates predominate. Therefore, the torque constraints are not approached. The optimal motion times for these examples are higher, 0.735 s and 1.5 s, respectively.

The optimal trajectories determined through the proposed method are not bang-bang in the controls. This is a consequence of the parametrization in the phase plane. However, as seen from the first example presented, the chosen parametrization alone causes a comparatively small increase in the motion time.

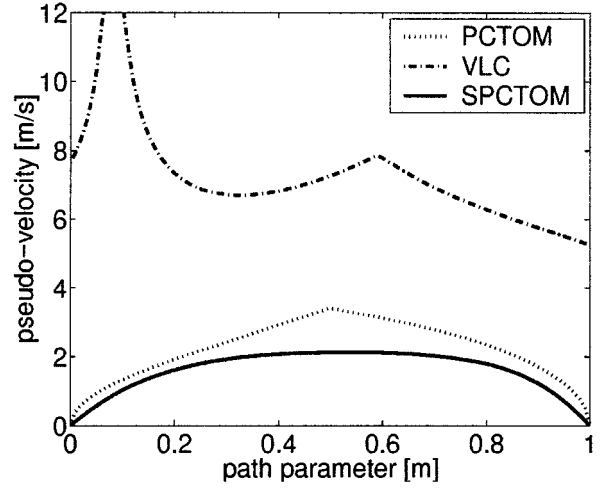
As expected, the more restrictive the limits on torque rates are, the higher the motion time is. The planning simulations, however, give no indication of the relationship between trajectory smoothness and the tracking performance of the controller. To establish tracking performance five simulations, followed by five experiments were performed.

4.2. Tracking Performance

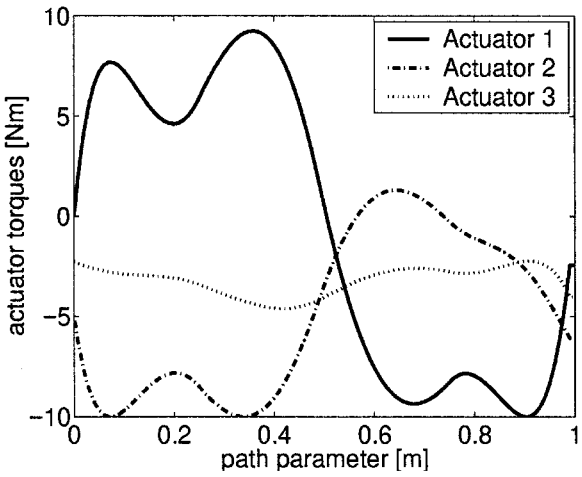
The two of the SPCTOM trajectories computed above, with “feasible” medium and low actuator torque rates, together with the PCTOM trajectory and an optimized quintic polynomial trajectory, have been implemented on a simulated model of the SCORBOT ER VII robot with friction controlled by a proportional-integral-derivative (PID) independent joint controller.



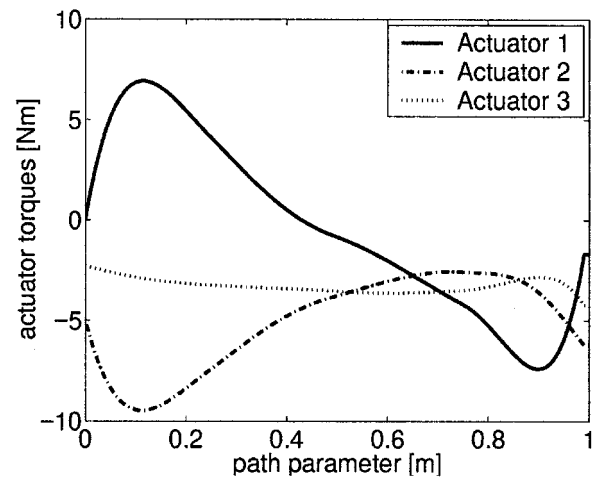
(a)



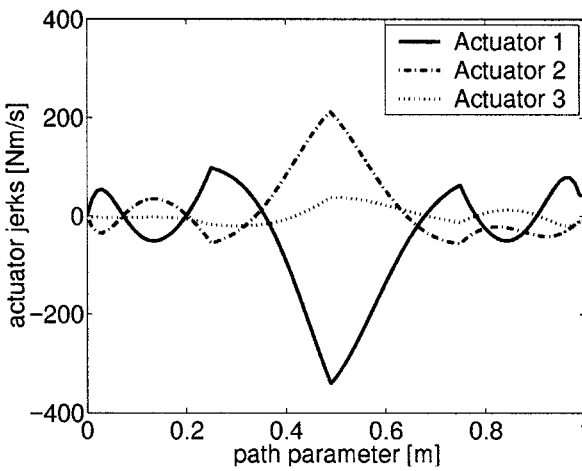
(a)



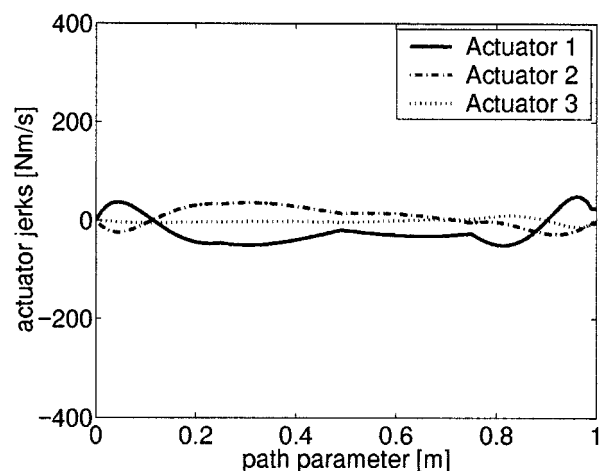
(b)



(b)



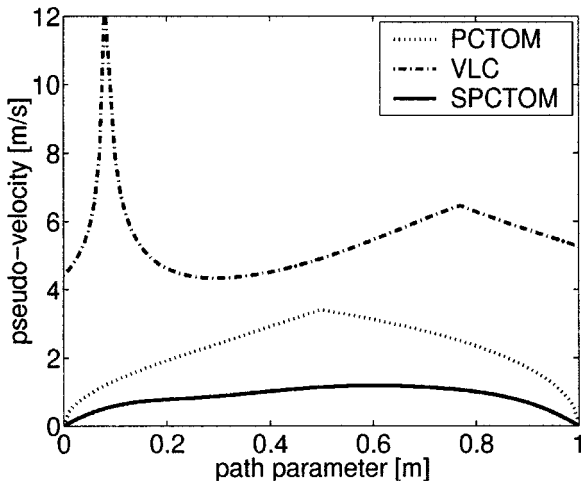
(c)



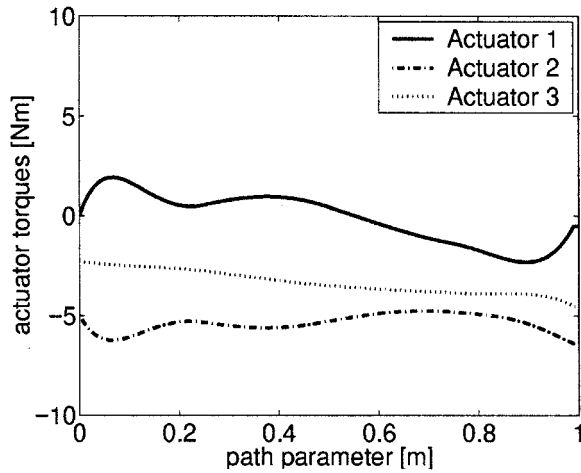
(c)

Figure 7. Example 1 (high torque rate limits).

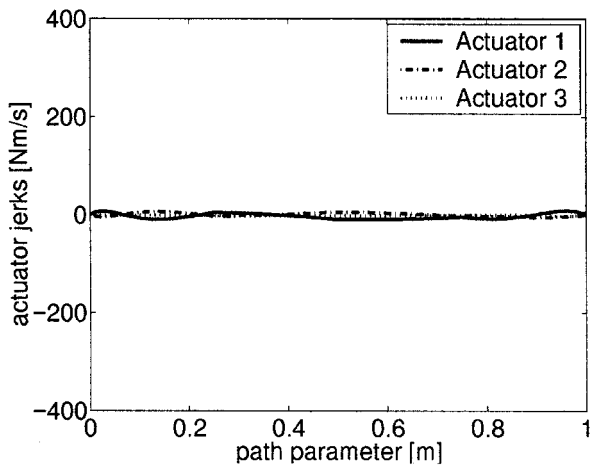
Figure 8. Example 2 (medium torque rate limits).



(a)



(b)



(c)

Figure 9. Example 3 (low torque rate limits).

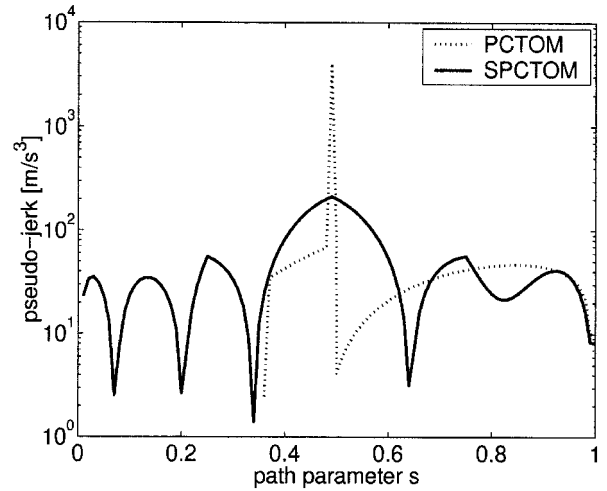
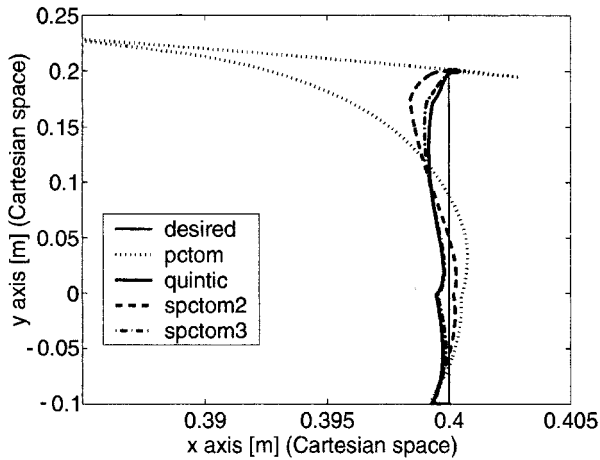


Figure 10. Absolute values of the torque rates for the SPCTOM in example 1 (solid lines) and PCTOM (dotted lines).

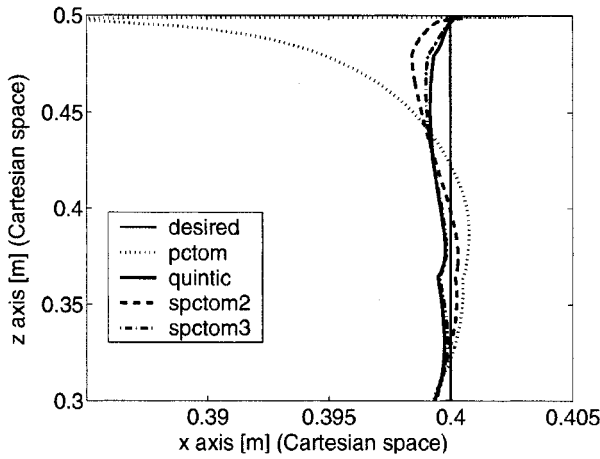
Both the robot model and the controller have been built in the MATLAB Simulink Toolbox.¹⁷ Friction has been modeled as Coulomb and viscous friction, with the Coulomb friction coefficients 2.0 Nm and the viscous friction coefficients 0.2 Nms for all three links. The controller has been tuned for critical damping and a rise time of 200 ms for a sampling frequency of 200 Hz. In the simulations, the actuator torques saturate at 10 Nm, which is the torque limit considered during planning.

The tracking performance of the PID controller for all four trajectories is plotted in Figure 11, while the planned and simulated actuator torques are plotted in Figs. 12–15. The results are summarized in Table III.

As seen in Figure 11, due to actuator torque saturation, the controller cannot keep the end-effector on the path when the torque rates are too high. This is the case with the PCTOM trajectory and the SPCTOM trajectory corresponding to torque rate limits of 100 Nm/s (labeled 'sptom2' in Fig. 11). This result shows that torque rate limits are extremely important for the ability of the system to track a planned trajectory, especially given inaccurately identified or modelled system dynamics. As expected, the smoother the trajectory, i.e., the lower the torque rate limits, the higher the tracking accuracy of the controller. For the PCTOM trajectory, the simulation predicts actuator saturation, which re-



(a)



(b)

Figure 11. Simulated controller tracking performance for the PCTOM, quintic, and SPCTOM trajectories.

sults not only in decreased tracking performance, but also in longer motion time (Table III).

The simulations show similar tracking performance for the SPCTOM trajectory with low torque rates and the quintic trajectory generated based on torque and velocity limits.¹ However, the SPCTOM trajectory takes 1.5 s, compared to 2 s for the quintic trajectory.

¹Quintic trajectories are completely specified by torque and velocity limits. The reported trajectory torque rate for the quintic trajectory depends on these limits.

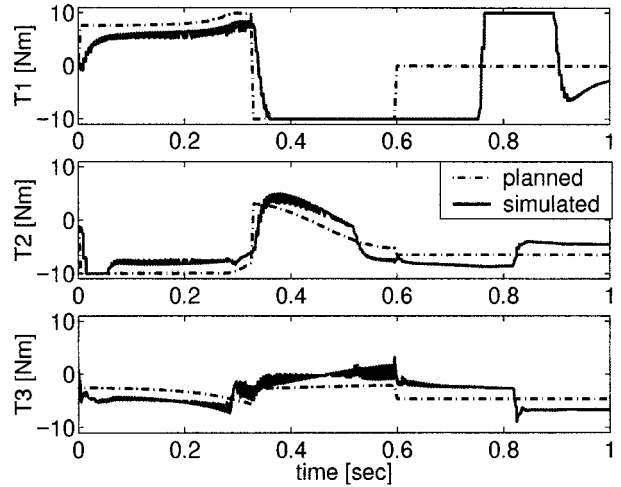


Figure 12. Desired and simulated torques for the PCTOM trajectory.

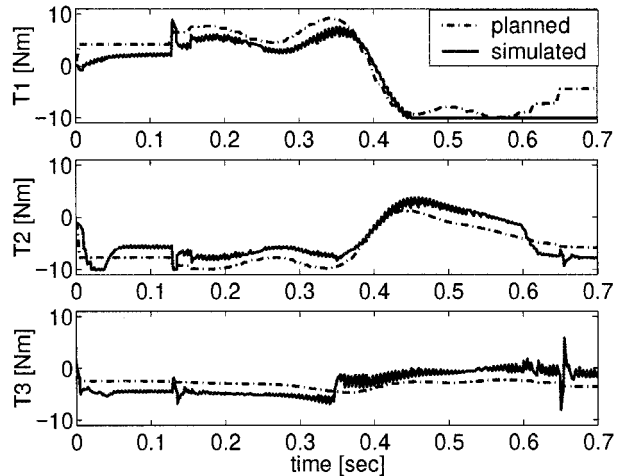


Figure 13. Desired and simulated torques for the SPCTOM trajectory (example 2—torque rate limits of 100 Nm/s).

5. EXPERIMENTS

All the above trajectories have also been implemented on the SCORBOT ER VII in the IAL at UBC. The robot is controlled by a TMS320C32 digital signal processing board, interfaced with two axis control cards, each capable of handling three axes simultaneously. An Open Architecture Real-Time operating system (ORTS)¹⁸ is used in the implementation of the control algorithm and in reading the pre-planned trajectories and feeding them to the

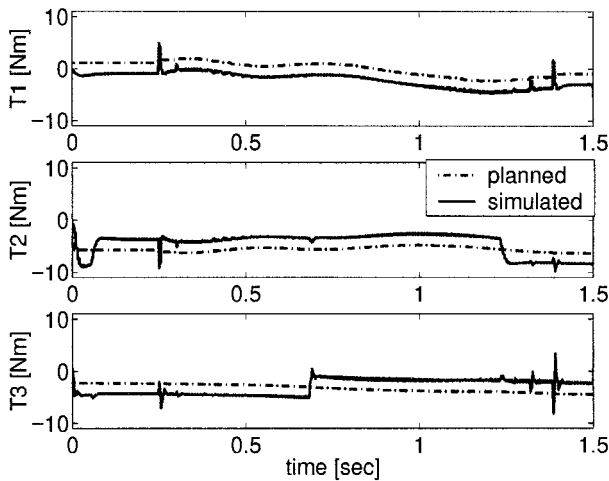


Figure 14. Desired and simulated torques for the SPCTOM trajectory (example 3—torque rate limits of 10 Nm/s).

control loop at the controller frequency. The axis control cards and the ORTS were developed by the Manufacturing Automation Laboratory (MAL), UBC. For the purpose of the experiments reported here, only the positional degrees of freedom of the robot are considered, thus the robot is treated as a 3-dof elbow manipulator with the kinematic and dynamic parameters given in Table I. A tuned, discrete PID algorithm is used to provide the control law. This setup simulates typical conditions in industry, where the robot is equipped with a closed architecture discrete PID independent joint controller.

The results of the experiments are plotted in Figures 16–19, and summarized in Table IV.

These experimental results support the simulation results. Namely, for high torque rate limits, the controller cannot keep the end-effector on the path. Figures 16, and 17 show that trajectories with high

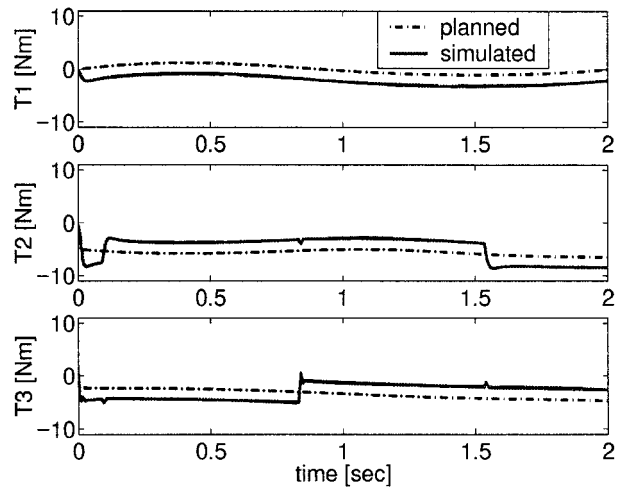


Figure 15. Desired and simulated torques for the quintic trajectory.

torque rates result in increased tracking errors, which, in turn, activate the controller, saturating the actuators. Whenever this happens, the end-effector leaves the path. Such a trajectory is an infeasible trajectory. For the case of the SCORBOT ER VII manipulator, torque rate limits less than one order of magnitude higher than the actuator torque limits are required to ensure that the end-effector follows the planned path. While this result is more restrictive for the torque rate limits than predicted by the simulations, it is not totally unexpected. Due to the large errors involved in modelling the system, one would expect that the simulation results would overestimate the system capabilities.

The experimental performance of the SPCTOM trajectory corresponding to the low torque rate limits, i.e., 10 Nm/s, is similar to its simulated performance. Thus, while being tracked by the controller with similar accuracy and effort as the quintic tra-

Table III. Simulated results for the PCTOM, SPCTOM, and quintic trajectories.

Trajectory	Torque rate limits [Nm/s]	Motion time [s]	Maximum tracking error [cm]	RMS tracking error		
				joint 1 [°]	Joint 2 [°]	joint 3 [°]
PCTOM	∞	0.90	1.98	1.54	0.31	0.37
SPCTOM 2	100	0.74	1.40	1.12	0.26	0.33
SPCTOM 3	10	1.50	0.64	0.53	0.12	0.16
Quintic	7	2.00	0.51	0.42	0.10	0.12

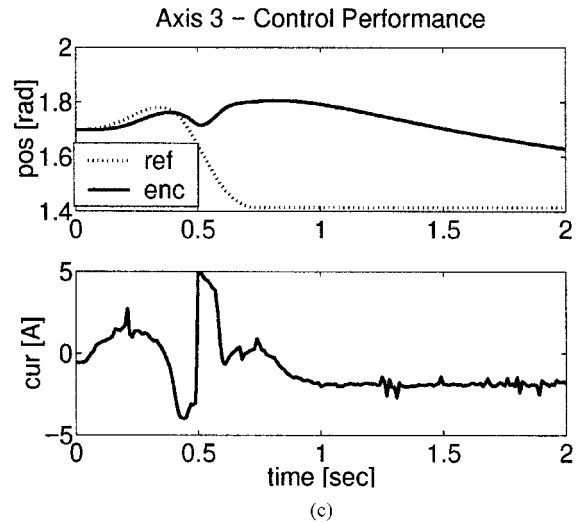
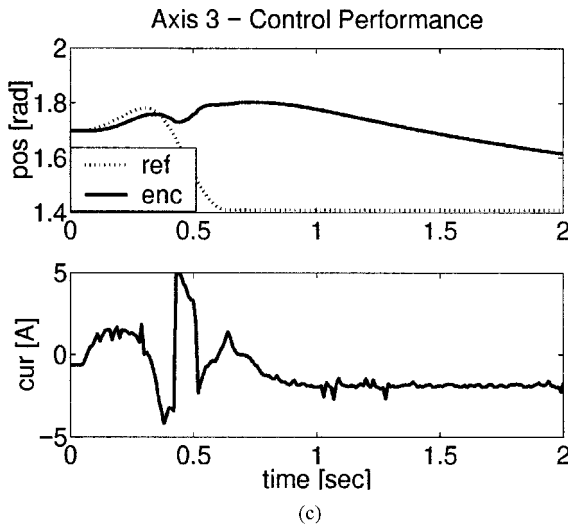
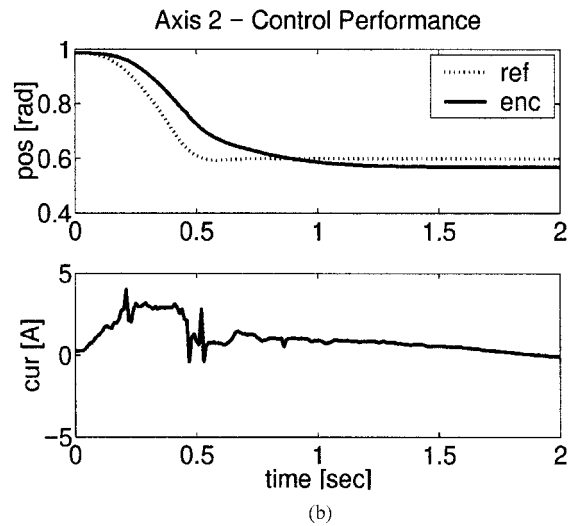
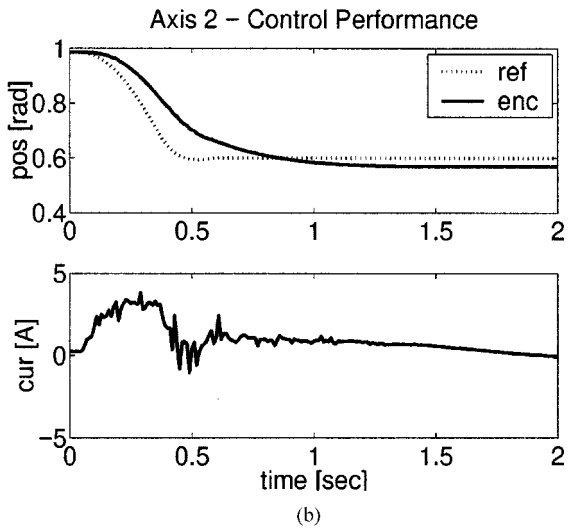
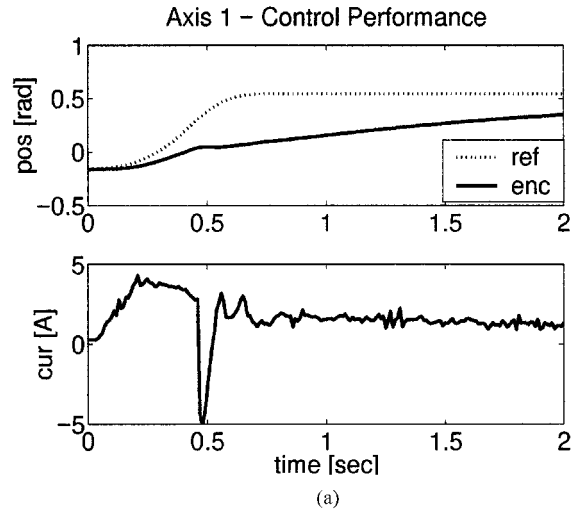
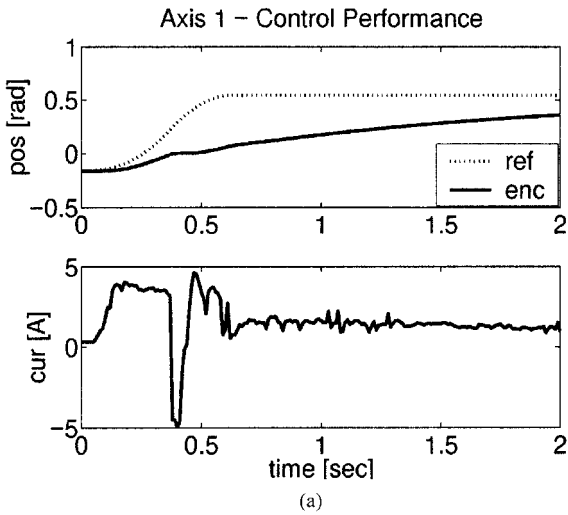


Figure 16. Experimental results for the PCTOM trajectory implemented on the SCORBOT ER VII.

Figure 17. Experimental results for the SPCTOM trajectory (example 2—torque rate limits of 100 Nm/s) implemented on the SCORBOT ER VII.

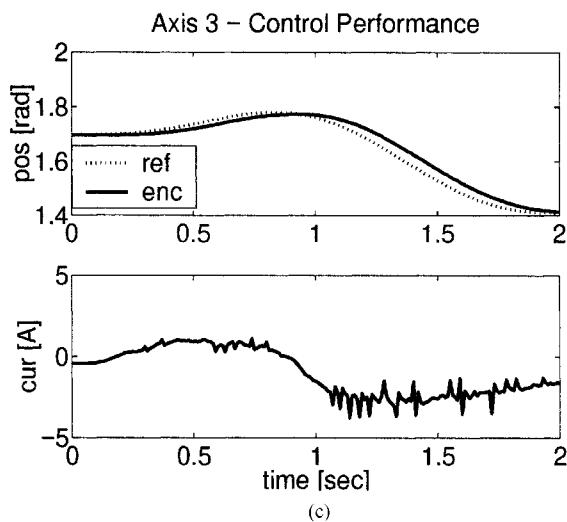
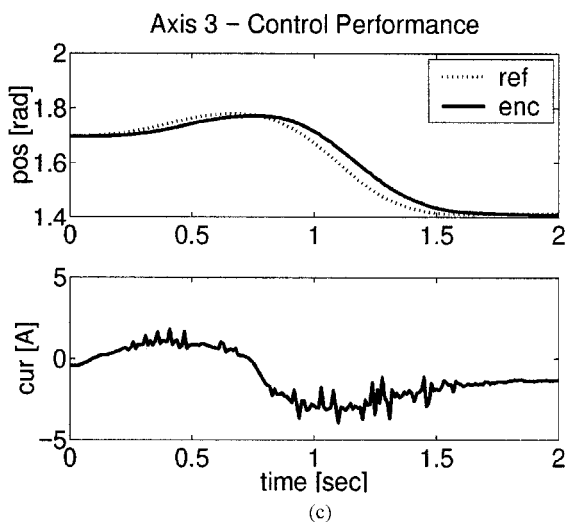
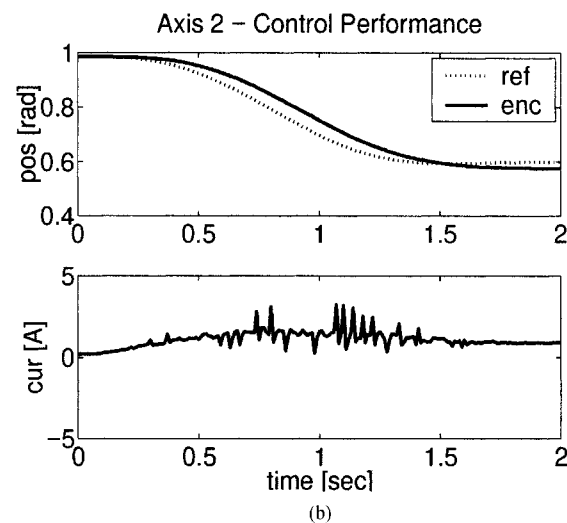
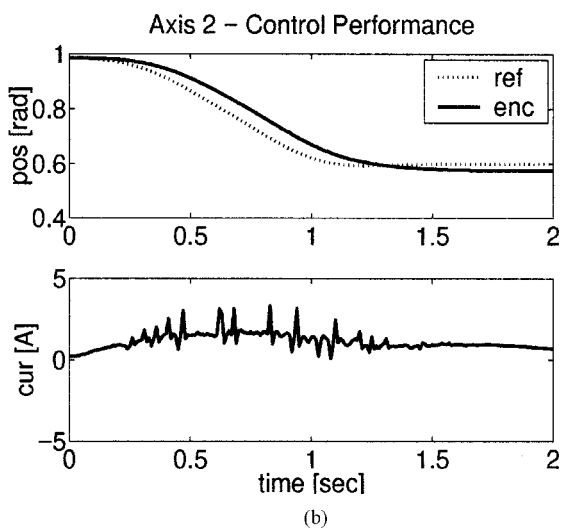
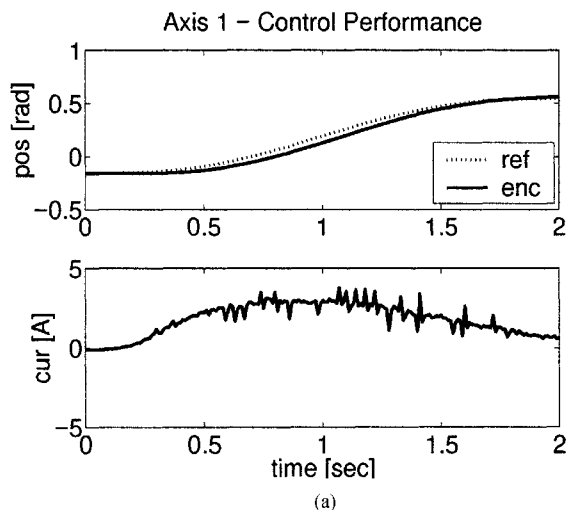
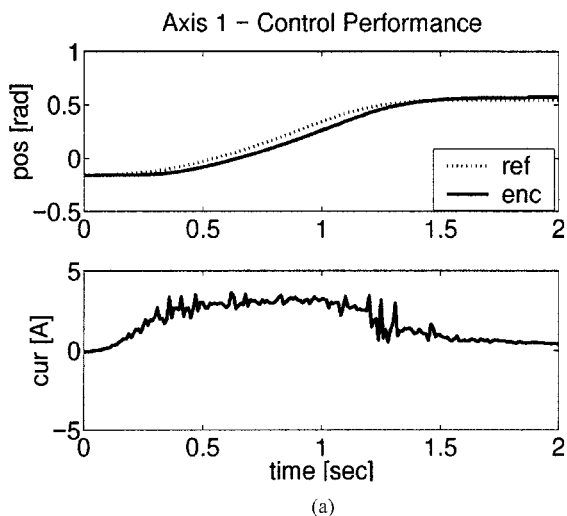


Figure 18. Experimental results for the SPCTOM trajectory (example 3—torque rate limits of 10 Nm/s) implemented on the SCORBOT ER VII.

Figure 19. Experimental results for the quintic trajectory implemented on the SCORBOT ER VII.

Table IV. Experimental results for the PCTOM, SPCTOM, and quintic trajectories under independent joint PID control.

Trajectory	Torque rate limits [Nm/s]	Motion time [s]	Maximum tracking error [cm]	RMS tracking error		
				joint 1 [°]	joint 2 [°]	joint 3 [°]
PCTOM	∞	4.0	14.0	17.5	3.1	15.8
SPCTOM 2	100	4.0	12.5	15.9	2.6	14.8
SPCTOM 3	10	1.5	3.1	2.6	1.9	1.5
Quintic	7	2.0	2.5	2.3	1.8	1.4

jectory, it results in reduced motion time (1.5 s compared to 2 s). This indicates that torque rate limits are preferable when determining smooth time optimal motions over global velocity and acceleration limits.

Experiments were also carried out using proportional-derivative (PD) plus gravity compensation control. The results are summarized in Table V and show the same correlation between the tracking accuracy and the torque rates along the trajectory.

6. CONCLUSIONS

A method has been presented for determining smooth and time-optimal path-constrained trajectories for robotic manipulators. The dynamics of the manipulator together with limits on the actuator torques and torque rates are considered. A base trajectory is constructed in the s - \dot{s} phase plane using parametrized cubic splines and a set of initial,

final, and knot-point conditions derived from PCTOM without torque rate limits. Thus, the optimal motion is obtained through an optimization of this base trajectory, subject to actuator torque and torque rate limits.

In planning simulations, the trajectory smoothness has a negative impact on the motion time, lower torque rate limits resulting in higher motion time. However, both controller simulations and experiments have shown that, in practice, trajectory smoothness has a positive effect on both the tracking performance of the controller and the actual motion time. Moreover, a smoothly planned trajectory can compensate for a poorly modeled robot system, which is often the case in industrial practice.

Compared to a quintic polynomial trajectory with velocity and acceleration limits, the SPCTOM trajectory results in a faster motion for similar tracking performance. Thus, torque rate limits are preferable when imposing a desired degree of trajectory

Table V. Experimental results for the PCTOM, SPCTOM, and quintic trajectories under PD plus gravity compensation control.

Trajectory	Torque rate limits [Nm/s]	Motion time [s]	Maximum tracking error [cm]	RMS tracking error		
				joint 1 [°]	joint 2 [°]	joint 3 [°]
PCTOM	∞	6.0	30.6	17.5	3.7	15.5
SPCTOM 2	100	6.0	26.3	6.9	3.3	15.1
SPCTOM 3	10	1.5	5.6	2.5	3.2	1.3
Quintic	7	2.0	4.3	2.1	2.5	1.2

smoothness over quintic polynomials, since they are not posture-dependent.

APPENDIX A

In the flexible tolerance method (FTM),¹⁵ the optimization problem,

$$\text{Minimize: } f(\mathbf{x}) \quad \mathbf{x} \in \mathbf{R}^n \quad (\text{A1})$$

$$\begin{aligned} \text{Subject to} \\ \text{constraints: } h_i(\mathbf{x}) = 0 \quad i = 1, \dots, m \quad (\text{A2}) \\ g_i(\mathbf{x}) \geq 0 \quad i = m + 1, \dots, p, \end{aligned}$$

is solved as the following simpler equivalent problem with only one constraint:

$$\begin{aligned} \min: \quad & f(\mathbf{x}) \quad \mathbf{x} \in \mathbf{R}^n \\ \text{subject to: } & \Phi^{(k)} - \mathcal{A}(\mathbf{x}) \geq 0. \end{aligned} \quad (\text{A3})$$

$\Phi^{(k)}$ is the value of the flexible tolerance criterion at the k th step of the optimization and it also serves as a criterion for the termination of the search, and \mathcal{A} is a positive functional of all the equality and/or inequality constraints of the original problem. The cost function $f(\mathbf{x})$ and the equality and inequality constraints in (A3) may be linear and/or nonlinear functions of the variables in \mathbf{x} . The value of the cost function is improved by using information provided by feasible points, as well as certain nonfeasible points called *near-feasible points*. The near-feasibility limits are made more restrictive as the search advances, until in the limit only feasible points are accepted.

In (A4) below, $\mathcal{A}(\mathbf{x})$ is used as a measure of the constraint violation, while Φ is selected as a positive decreasing function of the \mathbf{x} points in \mathbf{R}^n . For the SPCTOM,

$$\mathcal{A}(\mathbf{x}) = \begin{cases} \max_i g_i(\mathbf{x}) & \text{if } \exists_i \text{ such that } g_i(\mathbf{x}) \geq 1 \\ 0 & \text{otherwise,} \end{cases} \quad (\text{A4})$$

and

$$\Phi^{(k)} = \min \left\{ \Phi^{(k-1)}; \kappa \sum_{i=1}^{r+1} \|x_i^{(k)} + x_{\text{centr}}^{(k)}\| \right\} \quad (\text{A5})$$

with κ a constant.

The tolerance criterion is used to classify points in \mathbf{R}^n . At the k th step of the optimization, a point

$\mathbf{x}^{(k)}$ is said to be:

1. Feasible, if $\mathcal{A}(\mathbf{x}) = 0$.
2. Near-feasible, if $0 \leq \mathcal{A}(\mathbf{x}) \leq \Phi^{(k)}$.
3. Nonfeasible, if $\mathcal{A}(\mathbf{x}) > \Phi^{(k)}$.

A small value of $\mathcal{A}(\mathbf{x}^{(k)})$ implies that $\mathbf{x}^{(k)}$ is relatively near to the feasible region, and a large value of $\mathcal{A}(\mathbf{x}^{(k)})$ implies that $\mathbf{x}^{(k)}$ is relatively far from the feasible region.

On a transition from $\mathbf{x}^{(k)}$ to $\mathbf{x}^{(k+1)}$, the move is said to be feasible if $0 \leq \mathcal{A}(\mathbf{x}^{(k+1)}) \leq \Phi^{(k)}$, and nonfeasible if $\Phi^{(k)} \leq \mathcal{A}(\mathbf{x}^{(k+1)})$.

The FTM entails two independent optimizations: an outer minimization of the cost function $f(\mathbf{x})$ and an inner minimization of the violation of constraints $\mathcal{A}(\mathbf{x})$ whenever the minimization of $f(\mathbf{x})$ yields an infeasible point. The outer optimization of the motion time is implemented in this paper using the flexible polyhedron method (FPM).¹⁹ The FPM is a search in n dimensions where the polyhedron changes shape to match the changing shape of the surface. In the vicinity of a minimum the polyhedron shrinks, surrounding the minimum. Replacement of an infeasible point with a feasible or near-feasible one is done through a line search using interval halving.

The computational requirements of the algorithm are similar to those of a nonlinear optimization. In this case, the main overhead is represented by the evaluation of the constraint violation measure in Eq. (A4). This overhead is reduced by evaluating the actuator torque and torque rate limits violation directly rather than the state and control constraint violation.

This work has been supported by the National Sciences and Engineering Research Council of Canada and the Faculty of Graduate Studies at UBC. The helpful suggestions of Professor B. Benhabib of the Department of Mechanical and Industrial Engineering of the University of Toronto is greatly appreciated. Also, the assistance of Professor Y. Altintas and the graduate students in the MAL, UBC, during the experimental part of this work is gratefully acknowledged.

REFERENCES

1. J.E. Bobrow, S. Dubowsky, and J.S. Gibson, Time-optimal control of robotic manipulators along specified paths. *Int J Robotics Res* 4 (1985), 3–17.
2. F. Pfeiffer and R. Johanni, A concept for manipulator trajectory planning, *IEEE J Robotics Automat RA-3* (1987), 115–123.

3. Z. Shiller and H.H. Lu, Computation of path constrained time optimal motions with dynamic singularities, *ASME J Dyn Syst Meas Control* 114 (1992), 34–40.
4. Y. Chen and A.A. Desrochers, Structure of minimum-time control law for robotic manipulators with constrained paths, in *IEEE Int Conf Robot Automat* 1989, pp. 971–976.
5. J. Li, R.W. Longman, V.H. Schultz, and H.G. Bock, Implementing time optimal robot maneuvers using realistic actuator constraints and learning control, *Astrodynamics* 1998, RA-3 (1998), 115–123.
6. Z. Shiller, Time-energy optimal control of articulated systems with geometric path constraints, in *IEEE Int Conf Robot Automat* 1994, pp. 2680–2685.
7. C.S. Lin, P.R. Chang, and J.Y.S. Luh, Formulation and optimization of cubic polynomial joint trajectories for industrial robots. *IEEE Trans Automat Contr* AC-28 (1983), 1066–1074.
8. M. Tarkiainen and Z. Shiller, Time optimal motions of manipulators with actuator dynamics, in *IEEE Int Conf Robot Autom* 1993, pp. 725–730.
9. Z. Shiller, On singular time-optimal control along specified paths, *IEEE Trans Robot Automat* 10 (1994), 561–571.
10. Z. Shiller and S. Dubowsky, Time optimal path planning for robotic manipulators with obstacles, actuator, gripper, and payload constraints, *Int J Robot Res* 8 (1989), 3–18.
11. K.G. Shin and N.D. McKay, A dynamic programming approach to trajectory planning of robotic manipulators, *IEEE Trans Automat Contr* AC-31 1986, 491–500.
12. H.G. Bock and K.-J. Plitt, A multiple shooting algorithm for direct solution of optimal control problems, in *9th IFAC World Congress* 1984, pp. 1853–1858.
13. G. Leitman, *The calculus of variations and optimal control*, Plenum Press, New York and London, 1981.
14. D. Constantinescu, Smooth time optimal trajectory planning for industrial manipulators, Master's thesis, University of British Columbia, 1998.
15. D.M. Himmelblau, *Applied Nonlinear Programming*, McGraw-Hill, 1989.
16. The MathWorks, Natwik, Massachusetts, *Matlab User's Guide*, 1995.
17. The MathWorks, Natwik, Massachusetts, *Simulink Toolbox User's Guide*, 1995.
18. N.A. Erol and Y. Altintas, Open architecture modular tool kit for motion and process control, in *ASME International Mechanical Engineering Congress and Exposition*, ASME Publication MED, Dallas, Texas, 1997, pp. 15–22.
19. J.A. Nelder and R. Mead, A simplex method for function minimization, *Comput J* 4 (1964), 308–313.